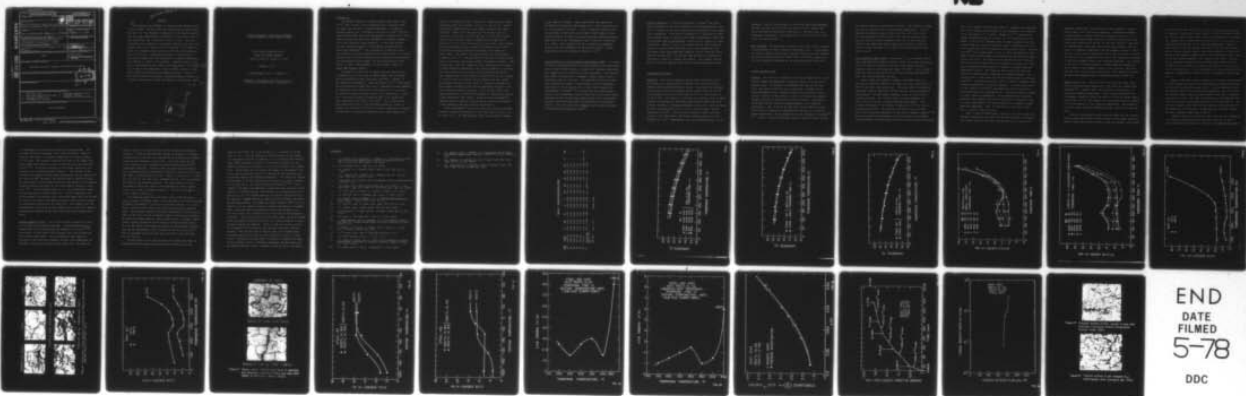


AD-A051 826

PENNSYLVANIA UNIV PHILADELPHIA DEPT OF METALLURGY AN--ETC F/G 11/6
EFFECT OF RESIDUAL IMPURITIES ON HYDROGEN ASSISTED CRACKING IN --ETC(U)
DEC 77 N BANDYOPADHYAY, C J MCMAHON N00019-77-C-0158

UNCLASSIFIED

| OF |
AD
A051826



END
DATE
FILMED
5-78
DDC

UNCLASSIFIED

SECURITY CLASSIFICATION OF THIS PAGE (When Data Entered)

AD A 051826

DDC FILE COPY

REPORT DOCUMENTATION PAGE		READ INSTRUCTIONS BEFORE COMPLETING FORM
1. REPORT NUMBER	2. GOVT ACCESSION NO.	3. RECIPIENT'S CATALOG NUMBER
4. TITLE (and Subtitle) Effect of Residual Impurities on Hydrogen-Assisted Cracking in High-Strength Steels,		5. DATE OF REPORT & PERIOD COVERED Final Report, for Period 8 Dec 1976 - 7 Dec 1977
7. AUTHOR(s) Nikhiles/Bandyopadhyay & Charles J./McMahon, Jr.		8. CONTRACT OR GRANT NUMBER(s) N00019-77-C-0158
9. PERFORMING ORGANIZATION NAME AND ADDRESS Department of Metallurgy and Materials Science, University of Pennsylvania, Philadelphia, Pennsylvania 19104		10. PROGRAM ELEMENT, PROJECT, TASK AREA & WORK UNIT NUMBERS
11. CONTROLLING OFFICE NAME AND ADDRESS U. S. Naval Air Systems Command Headquarters Washington, D.C.		12. REPORT DATE December 8, 1977
14. MONITORING AGENCY NAME & ADDRESS (if different from Controlling Office) Same		13. NUMBER OF PAGES 38 (237p.)
		15. SECURITY CLASS. (of this report) UNCLASSIFIED
		15a. DECLASSIFICATION/DOWNGRADING SCHEDULE
16. DISTRIBUTION STATEMENT (of this Report) Approved for public release, distribution unlimited		
17. DISTRIBUTION STATEMENT (of the abstract entered in Block 20, if different from Report) DDC MAR 27 1978 F		
18. SUPPLEMENTARY NOTES		
19. KEY WORDS (Continue on reverse side if necessary and identify by block number) 1. 4340-type steels 2. One-step temper embrittlement 3. Cryogenic impact tests 4. Intergranular fracture 5. Hydrogen-induced cracking 6. Hydrogen charging 7. Hydrogen-assisted cracking		
20. ABSTRACT (Continue on reverse side if necessary and identify by block number) See Attachment		

DD FORM 1473 JAN 73

EDITION OF 1 NOV 65 IS OBSOLETE

410408

SECURITY CLASSIFICATION OF THIS PAGE (When Data Entered)

TC

APPROXIMATELY EQUAL TO

Abstract

Intergranular embrittlement in 4340-type high strength steels (yield strength ~ 200 ksi) have been studied both at room temperature and 77 K. The toughness trough which is the manifestation of one-step temper embrittlement was absent in a high purity steel at room temperature, but it appeared in the 77 K tests. The room temperature test produced no intergranular fracture, but some intergranular facets were found in the 77 K specimens. For commercial steels, the toughness trough occurred in both the room temperature and the 77 K tests. Intergranular fracture in the high purity steel can be produced at room temperature by charging cathodically with hydrogen in sulfuric acid solution. Hydrogen-assisted cracking in the high purity steel showed a high K_{th} value (~ 72 ksi \sqrt{in}) in 1 atm H₂ at room temperature, which is about a factor of three greater than that observed in any commercial steels. Hence, in this type of steel the resistance to hydrogen-induced cracking can be greatly increased by bringing the impurity effects under control.

SP ROOT IN

SUB 24

ACCESSION NO.	
NTIS	
DOC	
UNANNOUNCED	
JUSTIFICATION	
BY	
DISTRIBUTION/AVAILABILITY CODES	
Dist.	
A	

EFFECT OF RESIDUAL IMPURITIES ON HYDROGEN-
ASSISTED CRACKING IN HIGH STRENGTH STEELS.

Final Report Submitted to the
NAVAL AIR SYSTEMS COMMAND
Under Contract No. N00019-77-C-0158

December 8, 1977

N. Bandyopadhyay and C.J. McMahon, Jr.

Department of Metallurgy and Materials Science
University of Pennsylvania, Philadelphia

Introduction

The residual impurities in high-strength alloy steels, such as AISI 4340, can play a very deleterious role, especially when the steels are exposed to certain environments, e.g. hydrogen, hydrogen-sulfide, etc. According to one point of view⁽¹⁾ one-step temper embrittlement (OSTE) and intergranular cracking at low stress intensity levels are due to the segregation of impurity elements to the prior austenite grain boundaries. It has been reported that the segregation appears to occur during austenitization, rather than tempering⁽¹⁾. This segregation of impurities lowers the cohesion at the grain boundaries and thereby results in an intergranular brittle fracture along the prior austenite grain boundaries. This intergranular embrittlement has been traditionally called "350'C" or "500'F" embrittlement or, more recently, "one-step temper embrittlement (OSTE)."

Grossman⁽²⁾ was the first to suggest that the carbides play an important role in this type of embrittlement, and he thought that intergranular fracture associated with OSTE is inherent in the tempering of martensite. Later on, Lement et al.⁽³⁾ investigated the microstructural changes that occur in martensite during tempering of high purity iron-carbon alloys containing 0.15 to 1.4% carbon. By careful electron microscopic studies, they showed that ϵ -carbide and a low carbon martensite containing about 0.25% carbon form after tempering at 300^o-400^oF (150^o-205^oC). The ϵ -carbide then progressively dissolves in the low-carbon martensitic matrix on tempering at 400^o-600^oF (205^o-315^oC), with the formation of elongated carbide films at martensitic boundaries and as both globular and

absent in the high-purity heat, whereas the commercial-purity heats containing added trace elements such as P, N, Sb, Sn, etc. showed the typical toughness trough in the tempering temperature range $\sim 300-350^{\circ}\text{C}$. Hence, they concluded that the impurity elements, especially P and N, play a significant role in 350°C embrittlement and that the structural changes accompanying the tempering of martensite are not solely responsible for this kind of embrittlement. Electron microscopic studies showed no difference in the carbide precipitation sequence between the high-purity and commercial-purity heats. The effects of P and N on OSTE were also reported by Banerji et al.⁽¹⁾ Kula and Anctil⁽⁷⁾ proposed a mechanism which involves an interaction between carbides and impurity elements. They proposed that, after the completion of the cementite precipitation at higher tempering temperatures, the alloying elements in cementite and ferrite would start to diffuse and redistribute themselves. They suggested that certain impurity elements which are more soluble in α -ferrite will be rejected from the carbide after the carbide precipitation and hence would result in a transient enrichment of these impurity elements in the ferrite immediately adjacent to the thin, elongated cementite platelets. This, in turn, would cause tempered martensite (or 350°C) embrittlement by lowering the ferrite-carbide-interfacial (FCI) energy. Later, Rellick and McMahon⁽⁸⁾ suggested that the impurity rejection during carbide precipitation is more important than after carbide precipitation.

Schulz and McMahon⁽⁹⁾ studied in detail the effect of alloying elements in temper embrittlement of AISI 3340 steel (3.5% Ni, 1.7% Cr, and 0.4% C). The embrittlement effects were studied by adding

various impurity elements. They reported that the addition of molybdenum eliminated the embrittlement due to step cooling for Sb, Sn, As, and Mn, but not for P. In the as-quenched condition, the fracture mode in 3340 steel with 600 ppm P showed complete intergranular fracture in both oil quenched and brine-quenched specimens. Auger analysis of the intergranular facets showed the segregation of P. Hence, they suggested that the segregation of phosphorus occurs at the grain boundaries in the austenite phase. Similar observations were also reported by Banerji et al⁽¹⁾.

Characterization of one-step temper embrittlement (OSTE). The nature of OSTE has been characterized by the measurement of room temperature charpy V-notch (RTCVN) energy as a function of tempering temperature for a tempering time of one hour at each temperature. The embrittlement (OSTE) is manifested by a toughness trough, usually within a temperature range of $\approx 200-400^{\circ}\text{C}$. The magnitude of the dip in this curve indicates the degree of embrittlement, and the temperature range where it occurs specifies the critical heat treatment for embrittlement. Grossman⁽²⁾ first showed that this embrittlement results in an intergranular fracture along the prior austenite grain boundaries and the fracture mode changes mainly from transgranular cleavage or microvoid coalescence to predominantly intergranular fracture. Also, the transition temperature goes through a maximum in the embrittling temperature zone⁽¹⁰⁾.

Effect of Mn and Si. It has been previously reported⁽¹⁾ that phosphorus segregates to the grain boundaries during austenitization, and the P is retained in the prior austenite grain boundaries during tempering of martensite. A low level of segregated P is sufficient in ultra high-strength steels to cause one-step temper embrittlement (OSTE) and also hydrogen-induced intergranular cracking at low stresses or stress intensities. Banerji⁽¹⁾ et al. also showed that the OSTE trough was absent in a pure Ni Cr Mo base 4340 steel at room temperature, but the energy trough reappeared when commercial levels of Mn and Si were added to the pure heat. The fracture mode was partly intergranular and partly a mixture of cleavage and rupture. This suggests that Mn and/or Si plays an important role in this intergranular embrittlement.

Experimental Procedure:

Materials. Five heats of vacuum-induction melted (VIM) high purity 4340 steels (nos. 840,841,842,843, and 846) were received from the Republic Steel Corporation Research Center. These heats were designed to reveal the effects of increasing the Mn content from 0.02 to 0.7% in the presence of low Si (0.01%) and of 0.27% Si in the presence of low Mn (0.02%). The purpose is to clarify the respective roles of these elements in promoting one-step temper embrittlement (OSTE) and intergranular cracking in a hydrogen atmosphere at low stress intensity levels. The heats were processed into 1½" x 4½" x L billets with a soaking temperature of 2150°F. They were then resoaked at 2000°F and cross rolled to 1.00" thick plates and finally straight rolled to a final thickness of 0.625". Subsequently, they were Blanchard ground to 0.50"

thickness. Heat B7 (VIM) and heat B2 (air melted and vacuum degassed) had been received earlier⁽¹⁾ from the General Electric Company Corporate Research and Development Center and J.T. Ryerson & Son, Inc., Pittsburgh, respectively. The compositions of the steels used in this study are given in Table I.

Heat Treatment. The usual heat treatment of this type of steel involves austenitization at $\sim 850^{\circ}\text{C}$ followed by quenching in oil. In the present case coarse, medium, and fine prior austenite grain sizes were obtained by one-hour austenitization at 1150°C , 950°C , and 850°C , respectively. This was followed by tempering for one hour between 100°C and 500°C .

Results and Discussion:

Hardness. The reduction in hardness for one hour tempering over a wide range of tempering temperatures is shown in Figure 1 for four of the Republic heats. The hardness is essentially the same for all four heats, the scatter being only over a small band. Although the as-quenched hardness value is governed primarily by the carbon content (which is similar in these heats), it may be noted that the tempered hardness increases as the Mn and Si contents increase. The high-Si, low Mn heat (no.842) shows the maximum hardness at all tempering temperatures. This is due to the fact that silicon addition retards the kinetics of tempering by enhancing the stability of ϵ -carbide to higher temperatures, and increasing the time of formation of cementite⁽¹¹⁻¹³⁾. Figure 2 compares the hardness values of heats 840 and B7 in the

fine grained condition (austenitized at 850°C). The hardness is almost the same for both the heats at all tempering temperatures. Figure 3 compares the hardness values of these two heats at a coarse grain size (austenitized at 1150°C); again it is same for both the heats. Thus, an increase in prior austenite grain size by increasing the austenitizing temperature does not make any difference in hardness values in either heat 840 or B7. Both of these heats have the same carbon content.

Room Temperature Impact Tests. Previously⁽¹⁾, it was reported that at room temperature the toughness trough is absent in an ultra-high-purity steel, but that the commercial 4340-type steels showed the typical toughness trough in the temperature range ~325°-350°C. Similar experiments have been carried out on the five heats obtained from Republic Steel (nos. 840,841,842,843, and 846).

Figure 4 shows the toughness troughs in the RTCVN energy as a function of tempering temperature for these five heats austenitized at 850°C for one hour (fine grain size). The figure shows the tempering temperature range of about 300°-350°C as the most severe condition of embrittlement. The OSTE energy trough was absent in the Mn-and-Si-free heat (no.840). The fracture energy increased gradually up to 250°C, then very steeply at higher tempering temperatures. This provides confirmation of the results of Banerji et al.⁽¹⁾ on the G.E. high purity heat (B7). The addition of Mn and/or Si to this high purity steel caused the appearance of the typical toughness trough.^(1,14) With increasing bulk concentration of Mn, the depth of the toughness trough increased, indicating that the steel was more and more embrittled.

This result suggests that Mn, and perhaps Si, promotes the segregation of P to the austenite grain boundaries even though the steel contains a very low amount of P ($< 0.010\%$). Kaneko et al.⁽¹⁵⁾ demonstrated strong interaction of Mn and Si with P in γ -Fe containing 12% Ni at 1000°C . From their⁽¹⁵⁾ demonstration, it might be expected that for typical commercial levels of Mn and Si found in 4340-type steel, most of the phosphorus would be segregated in the austenite phase. Recently, Clayton⁽¹⁶⁾ also reported that in a Ni Cr steel, segregation of phosphorus in the austenite phase was increased with the increasing amount of Mn in the steel. The effect of a Si addition on the OSTE characteristics (heat 842) shows that the minimum in the energy curve (most severe condition of embrittlement) is pushed to a higher tempering temperature ($\sim 350^{\circ}\text{C}$). This indicates that silicon slows down the kinetics of embrittlement by delaying the tempering process. This silicon effect is consistent with the observations made by Allten and Payson⁽¹¹⁾. They found an increase in the ϵ -carbide \rightarrow cementite transformation temperature with silicon additions. A similar observation was also made by Alstetter,⁽¹²⁾ who found that silicon stabilizes ϵ -carbide, and hence the transformation of ϵ -carbide to cementite occurred at higher tempering temperatures. The decomposition of low-carbon martensite into cementite and ferrite would also be retarded so that it occurs simultaneously with the dissolution of ϵ -carbide at higher tempering temperature. Thus, the addition of silicon only shifts OSTE to a higher temperature range.

Figure 5 shows the RTCVN energy curves for the coarse grain size specimens (austenitized at 1150°C for one hour and then oil quenched). The fracture energy of the coarse-grained material is lower at all

tempering temperatures, and the degree of embrittlement is slightly greater than in the fine-grained condition. Although the toughness in the material is reduced as the prior austenite grain size is increased, the energy trough indicative of OSTE was absent even in the coarse grain condition for the Mn + Si-free heat (no.840). Note that the embrittlement in the other heats occurs more gradually with the increase in tempering temperature, and the toughness trough is spread out over a wider range of temperature than in the fine-grain specimens. The effect of the Si addition in the case of the coarse-grain specimens is much more pronounced than in the fine-grain specimens. The minimum in the curve is certainly pushed to a higher tempering temperature, and the depth of the toughness trough is also increased, indicating that the steel is more severely embrittled. This indicates that both Mn and Si play important roles in the embrittlement of 4340 steel.

Impact tests at 77°K. Heats 840 and B7 were used for charpy impact tests at liquid nitrogen temperature (77°K) using the standard ASTM technique⁽¹⁷⁾. Figures 6 and 7 show the plots of CVN energy as a function of tempering temperature. Tests at room temperature show no toughness trough for either heat 840 or B7, but the trough appears in the tests at 77°K. The general level of fracture energy is reduced at 77°K, as expected, at all tempering temperatures. The minimum in the curve occurs around the temperature range 250°-270°C in both the heats.

Extensive fractographic studies have been done with the scanning electron microscope on the fracture surfaces of the broken charpy bars. Figure 8 shows the fracture surfaces of the fine grained (austenitized

at 850°C for one hour and then oil quenched) charpy specimens of heat B7 tempered at temperatures below (200°C), in (250°C) and above (300°C) the fracture energy trough. When tested at room temperature (no toughness trough), the fracture mode was totally microvoid coalescence (indicating ductile rupture) at all tempering temperatures. However, when tested at 77°K, the specimen tempered at 200°C and 300°C showed mostly cleavage fracture, whereas the specimen tempered at 250°C (the bottom of the toughness trough) showed a few intergranular facets, even in the fine-grained condition. This suggests that there is some impurity segregation along the prior austenite grain boundaries, but in order to see its effect, the impact tests had to be carried out at a very low temperature. At this temperature, the yield strength of the material is high, and this resulted in some intergranular brittle fracture.

Figure 9 shows the fracture surfaces of fine grained (austenitized at 850°C) charpy specimens of heat 840 tempered at temperatures below, in, and above the fracture energy trough. The room temperature fracture mode is ductile for all tempering temperatures, but in 77°K tests the fracture surface shows many intergranular facets for a tempering temperature of 250°C. Note that the percentage of intergranular fracture in this case is much higher than that in the purer heat B7. The Mn and Si content in heat 840 (which is almost 10 times than that of B7) might have an effect here. In addition, the P content in heat 840 may be somewhat higher than in heat B7.

Cryogenic impact tests were also done in the case of a commercial air-melted, vacuum-degassed 4340-type steel (heat B2). Figure 10 shows the plots of CVN energy as a function of tempering temperature

for fine-grained (austenitized at 850°C for one hour and then oil quenched) commercial steel (heat B2) for both room temperature and 77°K tests. The toughness trough was observed at both testing temperatures at around $\sim 350^{\circ}\text{C}$. At 77°K the level of fracture energy is decreased once again at all tempering temperatures, and there is simply a downward shift in the entire energy curve. Figure 11 shows the comparison of the fracture surfaces at both testing temperatures. In the tests at room temperature the specimen at the bottom of the toughness trough showed only a small amount of intergranular fracture. However, at 77°K the amount of intergranular fracture was increased. Note that heat B2 shows a much higher amount of intergranular fracture at 77°K than either heats B7 or 840 (Figures 8 and 9 vs 11).

Figures 12 and 13 show the plots of CVN energy as a function of testing temperature for the ultra-high-purity heat B7 and commercial heat B2 for two tempering conditions corresponding to the top and bottom of the toughness trough (Figures 6 and 10). In the case of the pure heat B7, the ductile-brittle transition temperature (at Δ fracture energy = 50%) is around the temperature range $\approx -130^{\circ}\text{C}$. The transition temperature is moved to the right, as expected, when the steel is embrittled (tempered at 250°C). This explains the observations of intergranular fracture in the 77°K tests. In the case of the commercial heat B2, the transition temperature is in the temperature range $\approx -130^{\circ}\text{C}$ in the embrittled condition (350°C tempering), but the 250°C temper condition shows a much higher transition temperature ($\sim -20^{\circ}\text{C}$). This effect is presumably due to the large difference in hardness between 350°C temper condition (47 Rc) and 250°C temper condition (52 Rc). Whereas in case of high-purity-heat B7, the hardness

difference between 200°C and 250°C temper conditions is only of the order of 1 Rc.

King et al.⁽¹⁸⁾ made some toughness measurements and fractographic observations on a quenched and tempered 0.6% carbon steel (composition: 0.57% C, 0.60% Mn, 0.18% Si, 0.022% S, and 0.0231 P). They observed that the strength levels and microstructures obtained in this 0.6% C steel over the range of tempering temperatures associated with the toughness minima (~570° - 665°K) were comparable with those of 4340 and similar low-alloy steels. They observed minima in the curves of K_{Ic} vs. tempering temperature at about 570°K (~297°C) for 273°K tests and 665°K (392°C) for 173°K tests. The fracture mode at the minima, as well as at all other tempering temperatures, was reported to be 100% transgranular cleavage. So, they concluded that the fracture path was transgranular with respect to the austenite grains and the martensite packets, and the toughness minima was not associated with any impurity segregation at the prior austenite grain boundaries.

To examine this viewpoint, low temperature impact tests were done on a plain carbon steel (SAE 1064). The composition of the steel is given in Table I. The tests were done with subsize charpy bars (0.35" square x 2.150"). The initial set of specimens was austenitized at 950°C for one hour and then oil quenched. This was followed by tempering in the temperature range 200°-450°C. Figure 14 shows the plot of CVN energy as a function of tempering temperature for steel SAE 1064 for the 77°K tests. It showed a toughness trough around ~400°C. The high energy value for 200°C tempering was suspected to be the effect of retained austenite. Therefore the heat treatment was slightly modified to eliminate the retained austenite. Immediately after

oil quenching, the specimens were placed in liquid nitrogen. This was then followed by tempering in the range 150^o-450^oC. Figure 15 shows the CVN energy vs. tempering temperature for these specimens in 77^oK tests. The toughness trough was observed in the temperature range around 350^oC, which is similar to the 4340-type steel observed before^(1,14). The fracture surfaces of the broken charpy bars were examined in the scanning electron microscope. The specimen at the bottom of the toughness trough showed intergranular facets, whereas for the 300^oC and 400^oC specimens, the fracture mode was mostly cleavage. The observation of intergranular fracture at the bottom of the toughness trough contradicts the report of 100% transgranular cleavage by King et al.⁽¹⁸⁾. In the specimen broken at 77 K, the intergranular facets were observed mostly near the notch area. At this temperature, the yield strength of the material goes up and hence makes the steel brittle. The plastic zone ahead of the notch tip becomes small and this results in intergranular failure near the notch area. This suggests that the OSTE observed in this type of plain carbon steel is due to the impurity segregation as observed in the case of 4340-type high strength alloy steels.

Hydrogen-induced cracking. The fracture mechanics approach has been used to study crack growth in hydrogen. A modified wedge-opening-loading (WOL) pre cracked specimen was employed in this work^(19,20). Semicircular, 5% face notches (side grooves) were used to guide the crack along a single plane. The self-loading of the sample was achieved by a bolt-and-tup arrangement and the crack propagation was recorded by the drop in load on the tup (load cell). An analog-to-

digital converter was used and the millivolt output was recorded by teletype. Because the modified WOL specimen was loaded to a constant displacement with the bolt, the load and the crack length were uniquely related by the compliance of the system. The crack length and the stress intensity K were calculated by using the Novak and Rolfe⁽¹⁹⁾ compliance calibration. Figure 16 shows the good agreement between their calibration and our experimental compliance calibration for steel 840 (850°C, 1h, OQ and 300°C, 1h, WQ). Figure 17 shows an a vs. t curve for this steel at 23°C and 1 psig. hydrogen pressure. The crack length was found to vary smoothly with time. The crack growth rates were determined by taking the slopes of the approximately linear segments of the a vs. t plot, as shown in Figure 17. The $\log V (= \log \frac{da}{dt})$ vs. K curve is shown in Figure 18.

The following points are to be noted: First, steel 840 shows a high K_{th} value (72 $\text{ksi}\sqrt{\text{in}}$), which is less than that (120 $\text{ksi}\sqrt{\text{in}}$) observed by Banerji and McMahon⁽¹⁾ in the case of heat B7; however, it is still about a factor of three greater than that observed in any commercial steel. This finding confirms the previous conclusion⁽¹⁾ that the resistance of this type of steel to hydrogen-induced cracking can be greatly increased by bringing impurity effects under control. Secondly, fractographic studies (Figure 19) of the hydrogen-induced fracture surface of steel 840 showed a much higher percentage of intergranular fracture than the few intergranular facets observed in the case of heat B7⁽¹⁾. This is presumably due to the fact that steel 840 is less pure than heat B7 (Table I).

The next phase of this investigation will include experiments on hydrogen-assisted cracking on heats 841 (high Mn and low Si), 842

(high Si and low Mn), 843 (0.09% Mn and 0.01% Si) and 846 (0.23% Mn and 0.01% Si). Since the high purity heat 840 showed a large amount of intergranular fracture in hydrogen, it is worth doing some scanning Auger (SAM) experiments in order to investigate quantitatively the amount of segregation of impurities at the prior austenite grain boundaries. We have been able to increase the amount of intergranular fracture in ultra-high-purity heat B7 by charging the SAM (scanning Auger microprobe) samples with hydrogen cathodically. The sample was charged with hydrogen in 4% H_2SO_4 solution for 30 minutes at a current density of 0.02 amps per sq. in, using platinum as the anode^(21,22). After charging, the sample was immediately rinsed with water and then cadmium plated in a CdO-NaCN bath for 30-40 minutes at a current density of 0.2 amps per sq. cm. The cadmium anode was used and the plating bath was not agitated. Cadmium plating was done to prevent hydrogen from diffusing out during baking. The sample was finally baked at 140°C for 10-11 minutes in an air furnace to obtain a uniform distribution of hydrogen. Then, a slow bend test was carried out with an Instron machine at a very slow strain rate ($\sim 0.0002''/\text{min}$) to allow time for the hydrogen to diffuse in. The fracture surface of the broken sample was then examined under the scanning electron microscope, and a high percentage of intergranular fracture was observed. Figure 20 shows the fracture surface of the sample of B7 fractured by the slow bend test after hydrogen charging. This suggests that we would be able to do scanning Auger microprobe analysis, even for the ultra-high-purity steel, by using either a hydrogen pre-charged sample (as above) or breaking the sample inside the Auger system in a hydrogen atmosphere and then pumping out the hydrogen from the system. Assembly of this set up is in progress.

REFERENCES

1. S.K. Banerji, H.C. Feng and C.J. McMahon, Jr., Final Report to the Naval Air Systems Command under contract No.N00019-C-76-0298, Dec. 8, 1976; also Met. Trans. A (in press).
2. M.A. Grossman; Trans. AIME, 167, 39, (1946).
3. B.S. Lement, B.L. Averbach, and M. Cohen; Trans. ASM, 46, 851, (1954).
4. L.J. Klingler, W.J. Barnett, R.P. Frohberg, and A.R. Troiano; Trans. ASM, 1954, vol.46, p.1557.
5. H. Schrader, H.J. Wiester, and H. Shiepmann; Archiv Eisenhüttenwesen, 1950, 21, p.21-27.
6. J.M. Capus, and G. Mayer, Metallurgia, 62, 133, (1960); J. Iron Steel Inst., 196, 255, (1958); J. Iron Steel Inst., 201, 53, (1963).
7. E.B. Kula, and A.A. Anctil; J. of Matls., ASTM, 4, 817, (1969).
8. J.R. Rellick, and C.J. McMahon; Met. Trans., 5, 2439, (1974).
9. B.J. Schulz, and C.J. McMahon, Jr., in "Temper Embrittlement in Alloy Steels," ASTM STP 499, p.104, (1972).
10. R.L. Rickett, and J.M. Hodge; Proc. ASTM, 1951, vol.51, p.931.
11. A.G. Allten, and P. Payson; Trans. ASM, 45, 498, (1953).
12. C.J. Alstetter, M. Coehn, and B.L. Averbach; Trans. ASM, 55, 287, (1962).
13. W.S. Owen; J. Iron Steel Inst., vol.177, p.445, (1954).
14. N. Bandyopadhyay, and C.J. McMahon, Jr.; First Quarterly Report to the Naval Air Systems Command under contract No.N00019-76-C-0298, March 8, 1977.
15. H. Kaneko, T. Nishizawa, K. Tamaki, and A. Tanifuji; J. Japan Inst. of Metals, (1965), 29, p.166.
16. J.Q. Clayton; Ph.D. Thesis, Cambridge University, 1977.
17. 1973 ASTM standard, part 31, E 23-72, p.277.
18. J.E. King, R.F. Smith, and J.F. Knott; paper presented in Fourth International Conference on Fracture, Waterloo, Canada, Fracture 1977, vol.2, ICF4.
19. S.R. Novak, and S.T. Rolfe; J. Materials, 4, 701, (1969).

20. S.K. Banerji, and C.J. McMahon, Jr., Final Report to the Naval Air Systems Command under contract No.N00019-75-C-0125, October 1, 1975.
21. H.H. Johnson, J.G. Marlet, and A.R. Troiano; Trans. Met. Soc., AIME, vol.212, p.528, (1958).
22. E.A. Steigerwald, F.W. Schaller, and A.R. Troiano; Trans. Met. Soc., AIME, vol.215, p.1048, Dec. 1959.

Table I: Chemical Compositions (wt%)

<u>Heat</u>	<u>Steel</u>	<u>C</u>	<u>Mn</u>	<u>Si</u>	<u>P</u>	<u>S</u>	<u>Ni</u>	<u>Cu</u>	<u>Cr</u>	<u>Mo</u>	<u>Al</u>	<u>V</u>	<u>Cb</u>
840	4340 VIM	0.37	0.02	0.01	<.010	0.003	1.84	0.01	0.82	0.22	<.01	-	-
841	4340 VIM	0.38	0.72	0.01	<.010	0.005	1.83	<.01	0.82	0.26	<.01	-	-
842	4340 VIM	0.38	0.02	0.27	<.010	0.005	1.82	0.01	0.85	0.30	<.01	-	-
843	4340 VIM	0.36	0.09	0.01	<.010	0.005	1.81	0.01	0.89	0.28	<.01	-	-
846	4340 VIM	0.37	0.23	0.01	<.010	0.005	1.78	<.01	0.83	0.27	<.01	-	-
B2	4340 AM	0.39	0.68	0.08	0.009	0.016	1.72	-	0.73	0.22	0.046	0.05	0.04
B7	High Purity VIM NiCrMo base	0.37	0.007	0.002	0.003	0.003	1.82	0.002	0.81	0.25	<.001	-	-
	SAE 1064	0.64	0.70		<0.040	<0.050							

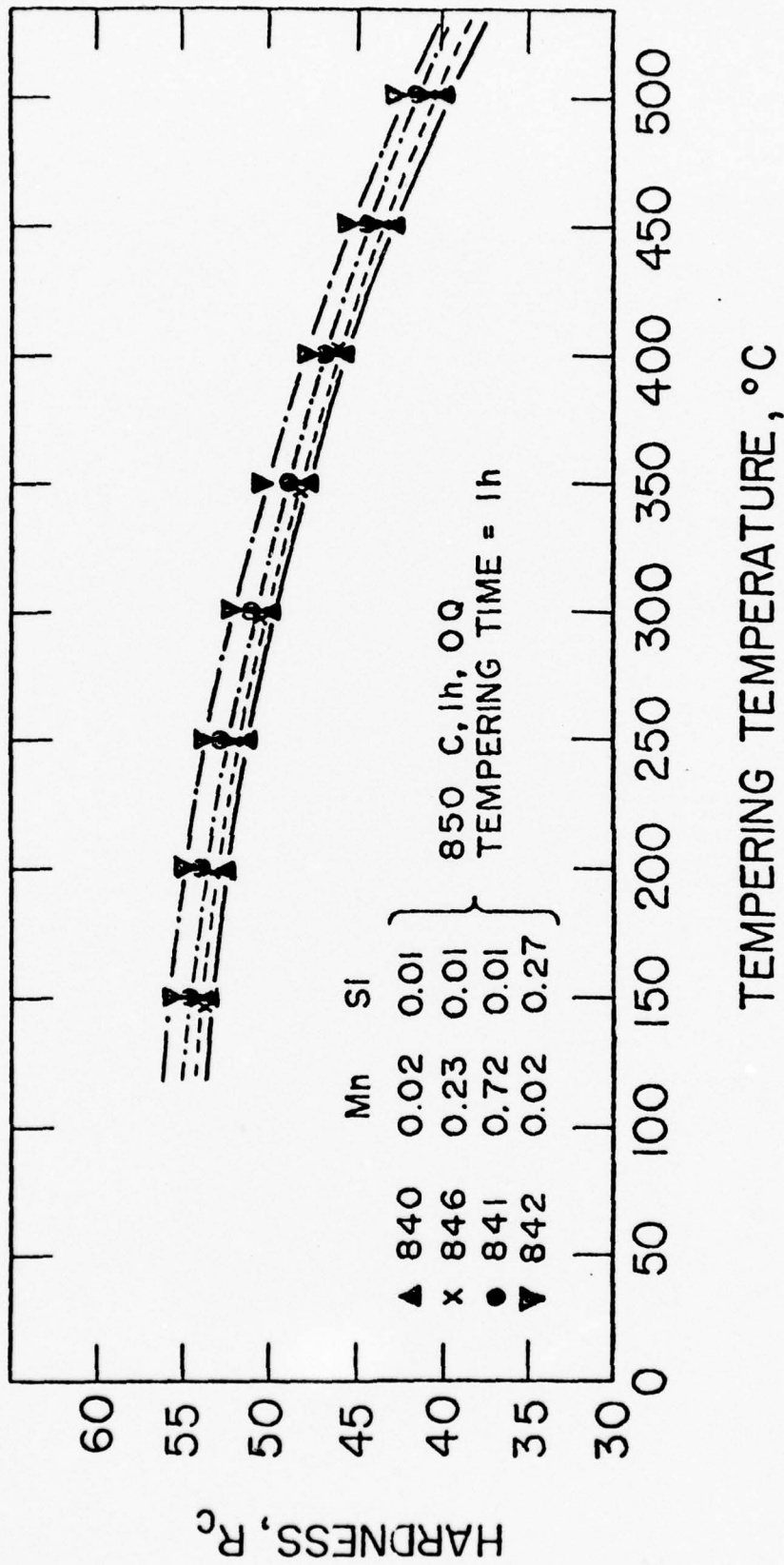


FIG-1

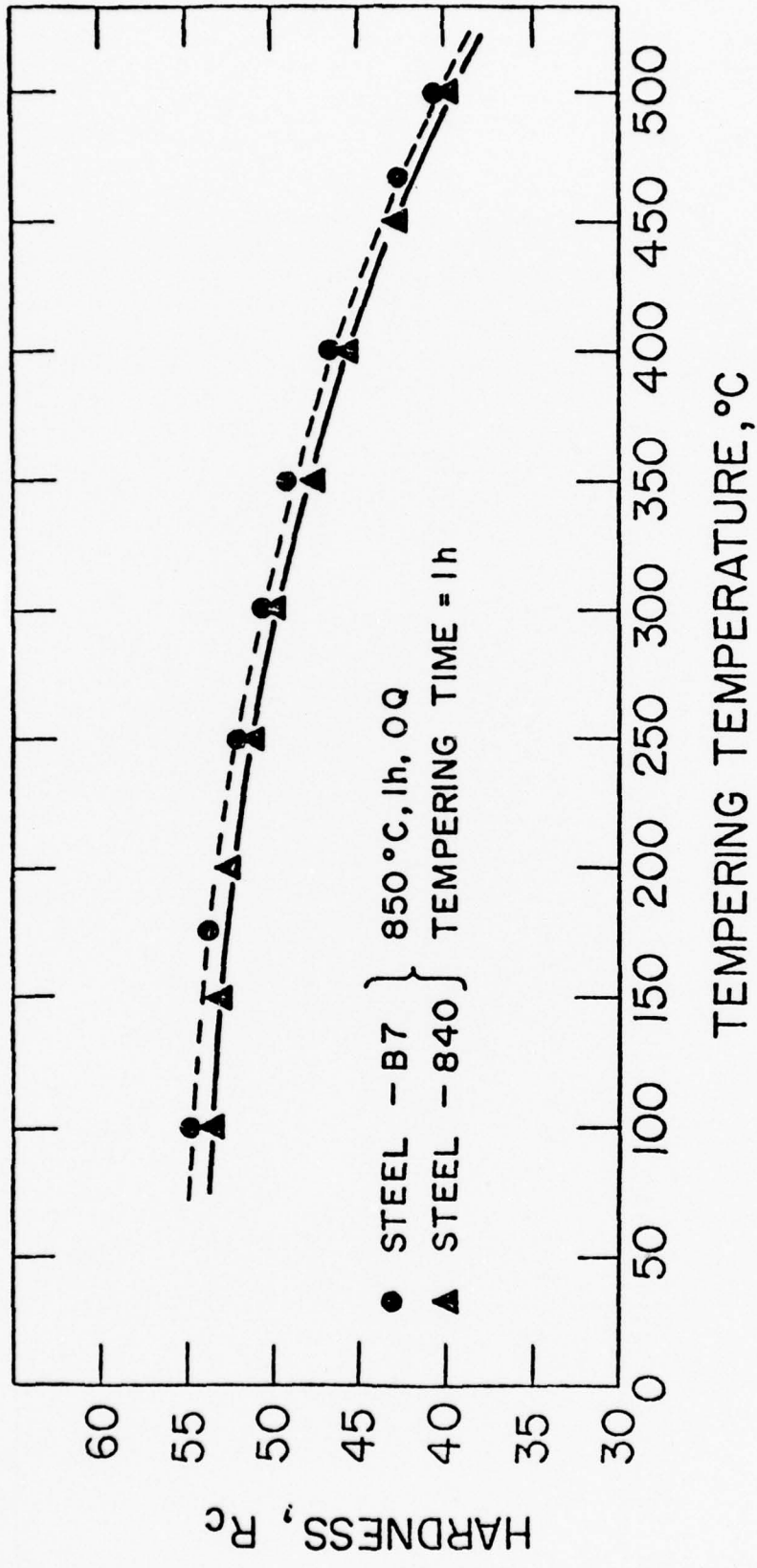


FIG. 2

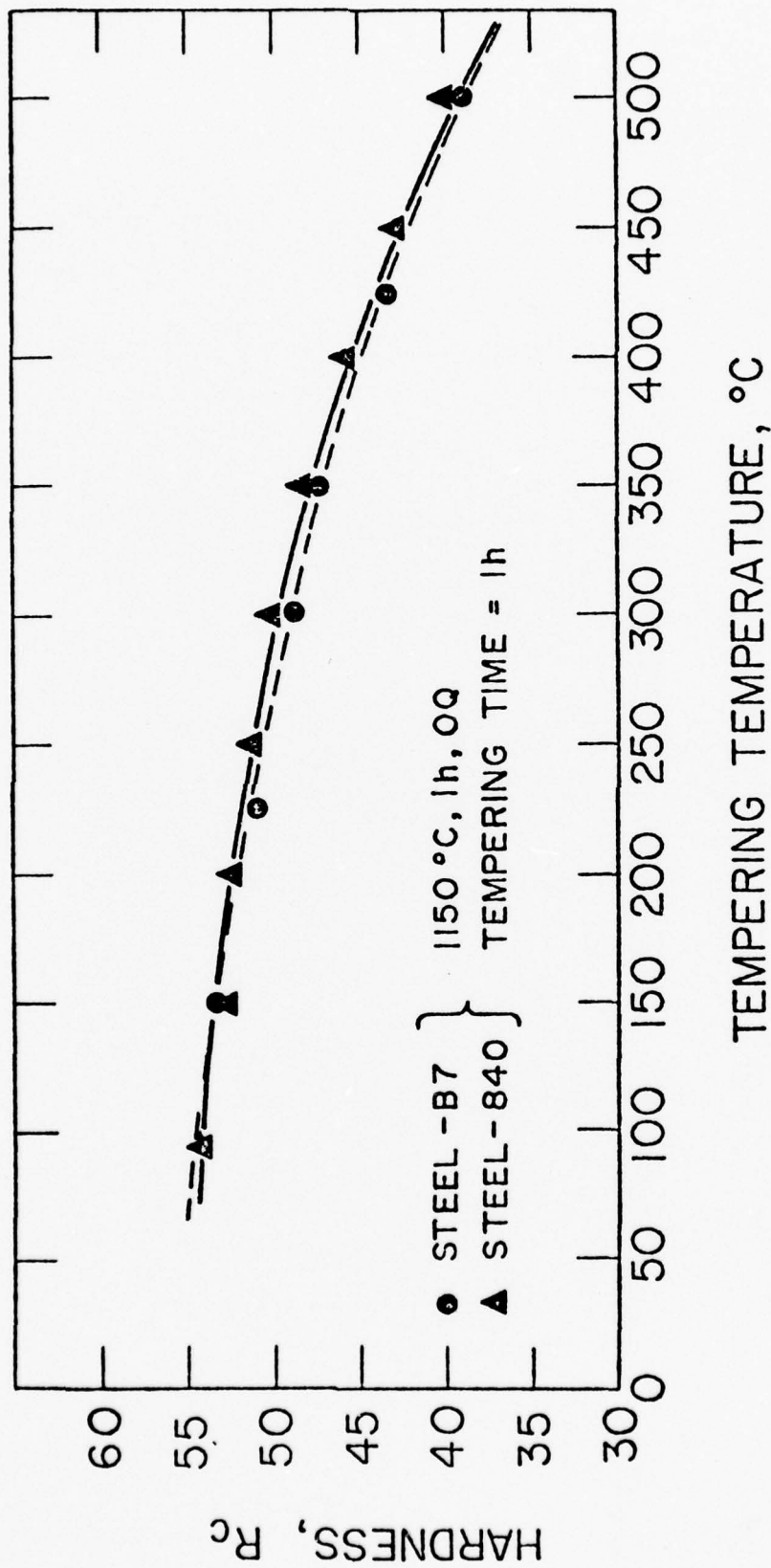


FIG-3

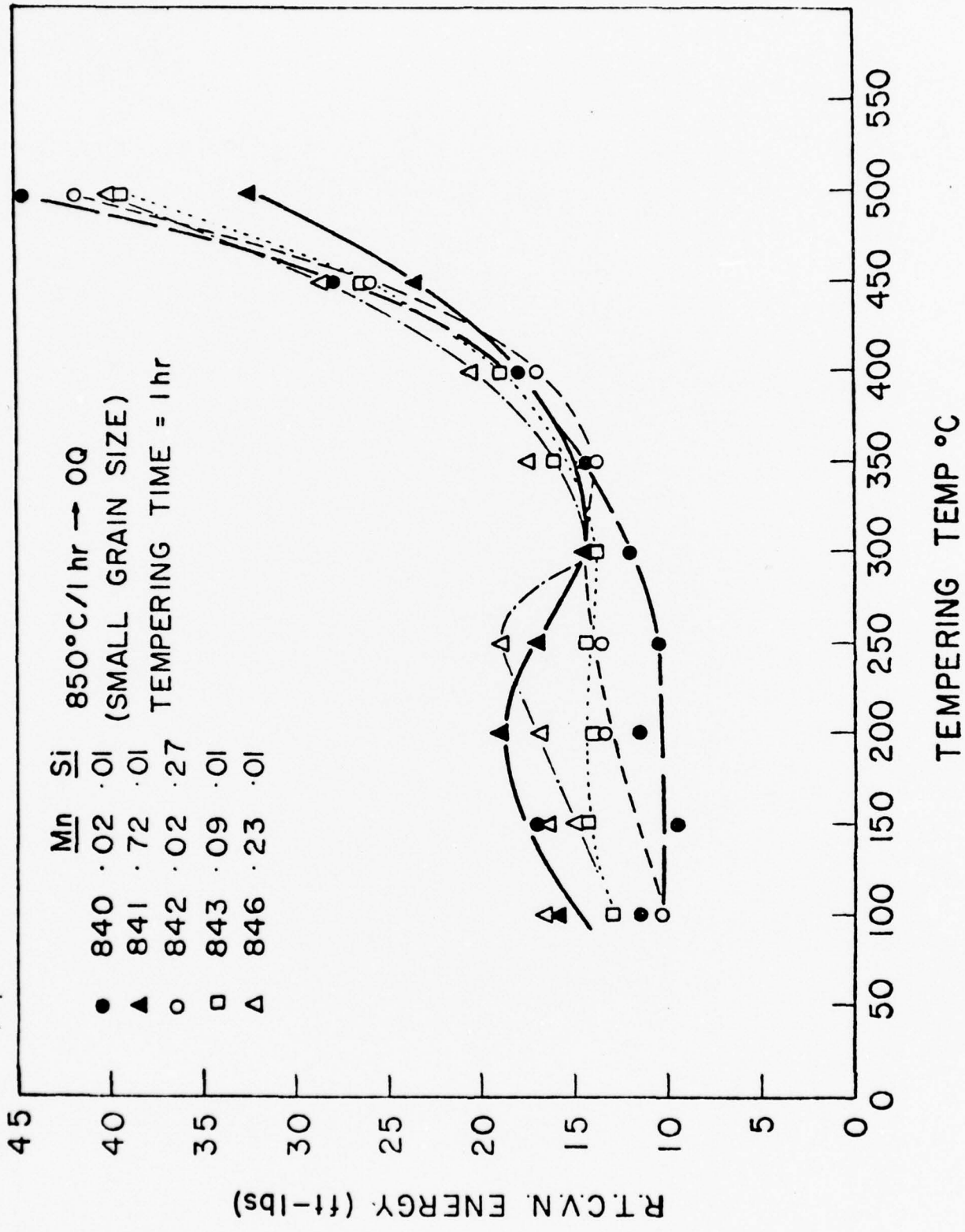


FIG-4

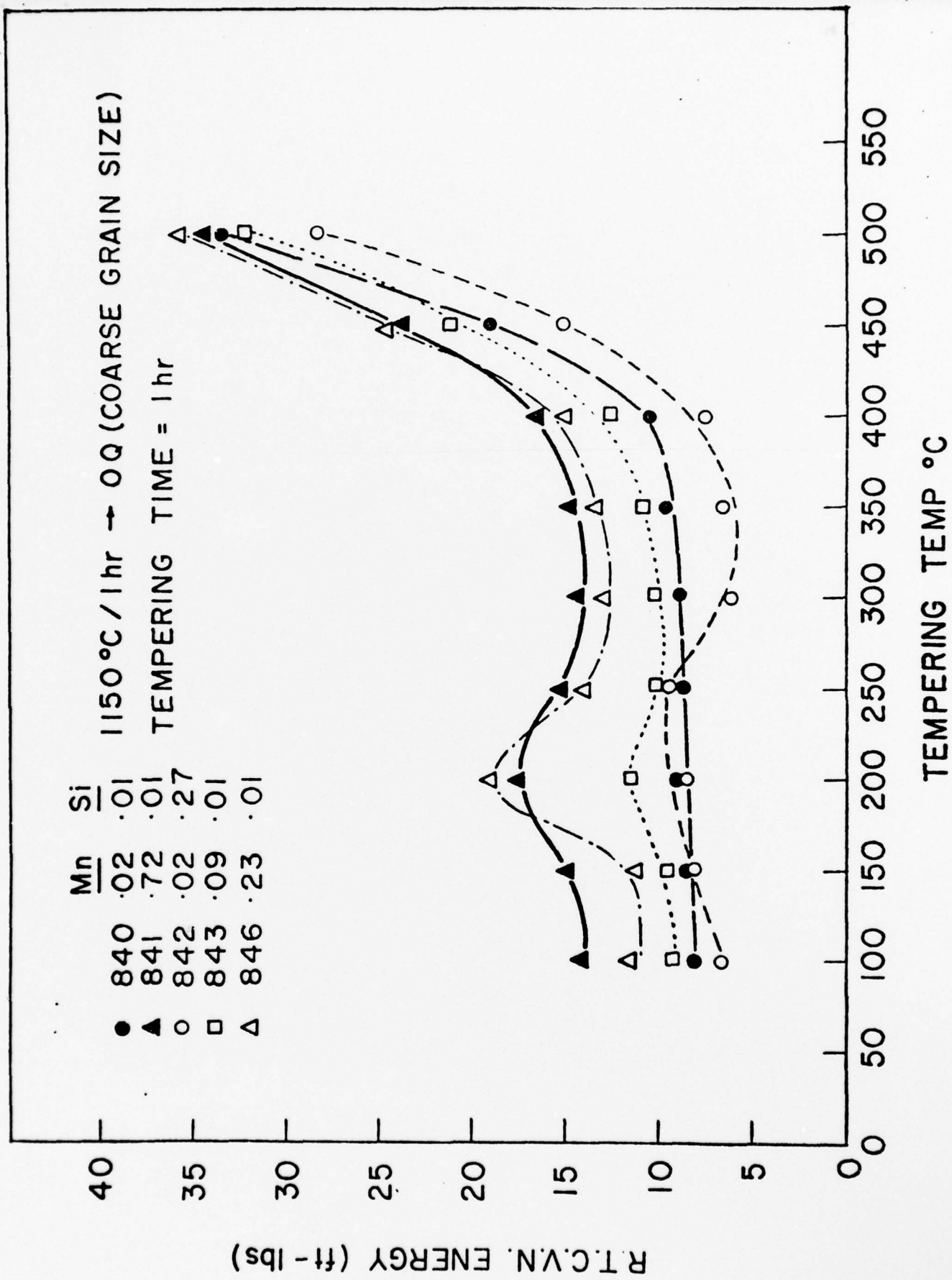


FIG-5

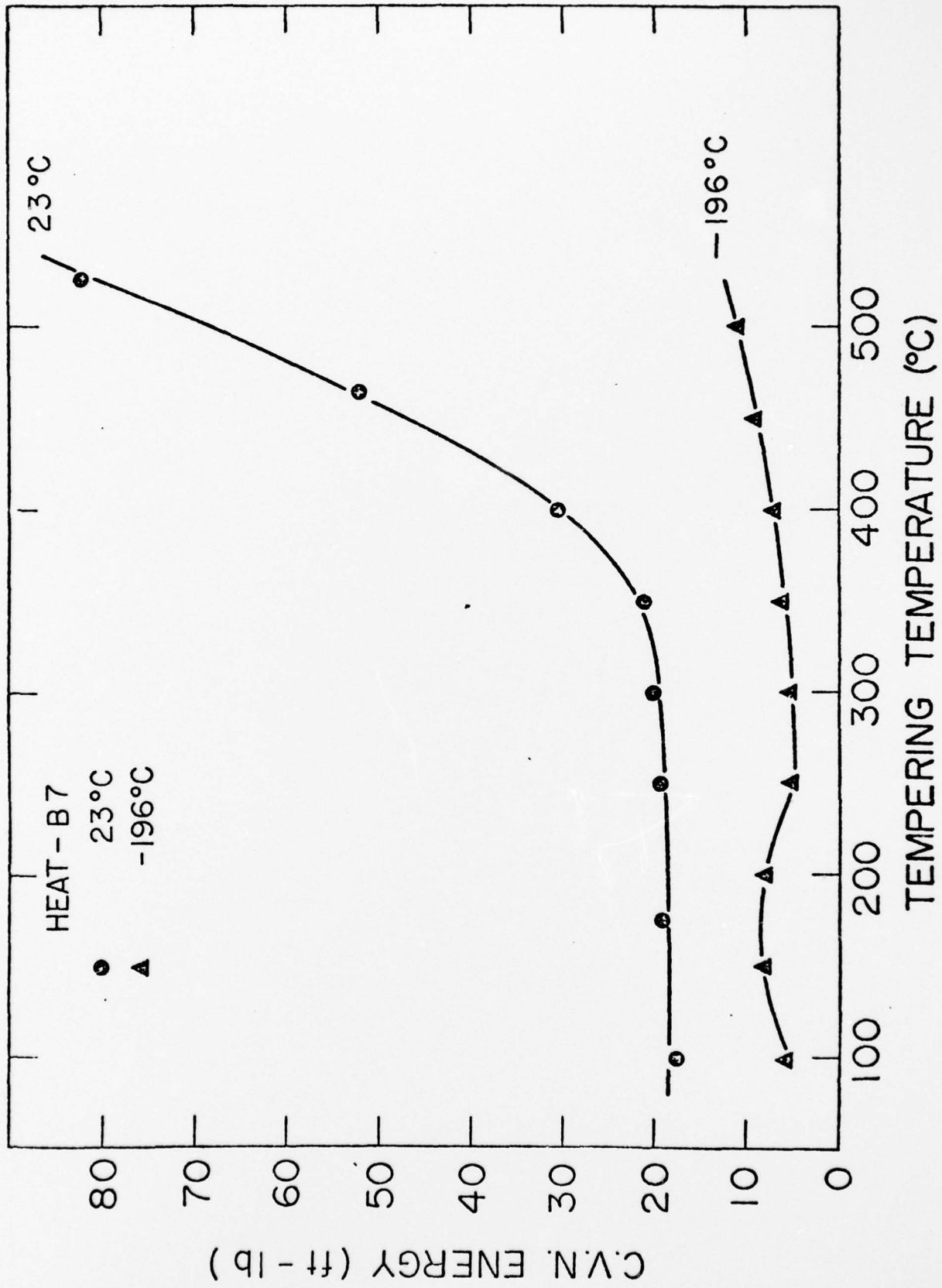


FIG-6

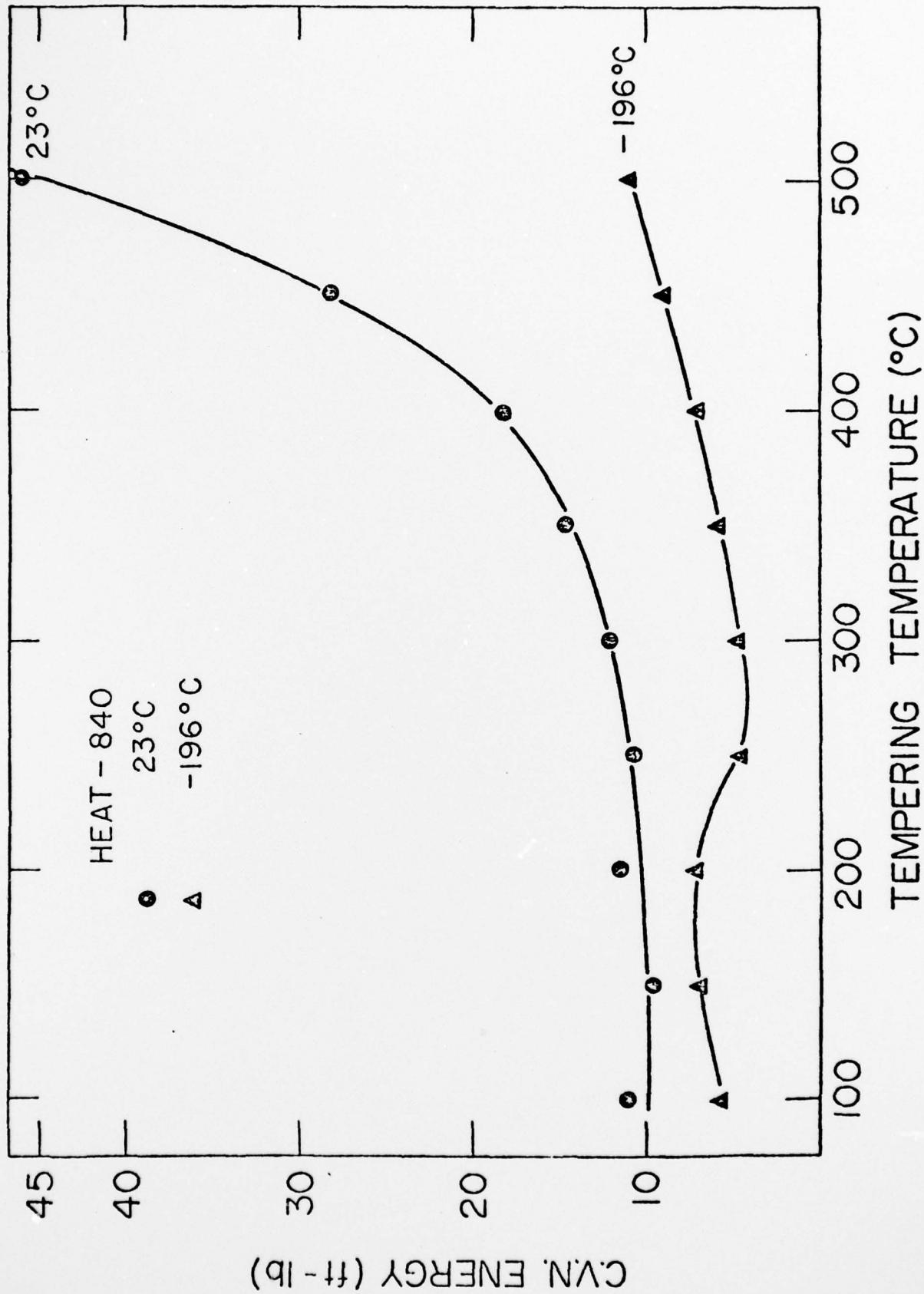
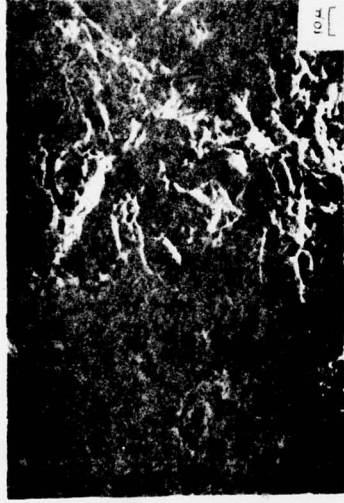


FIG.-7

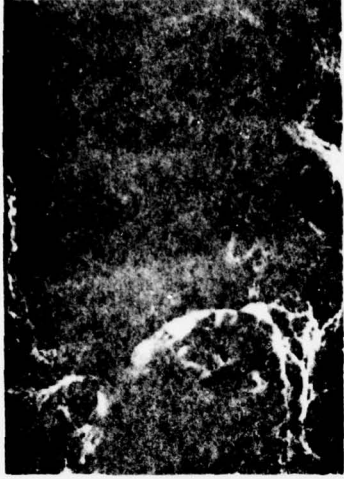
TEMPERED AT : 200°C



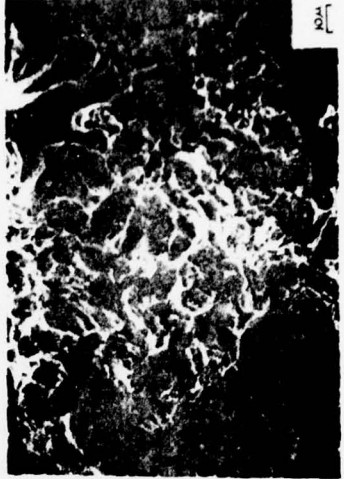
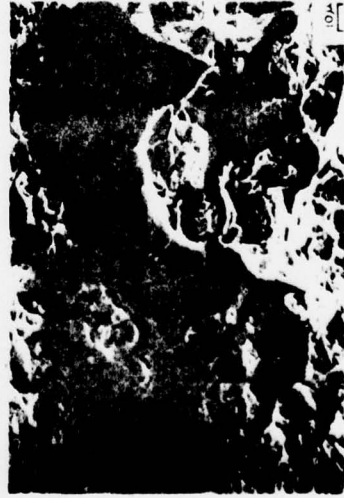
250°C



300°C



TESTED AT ROOM TEMPERATURE (23°C)



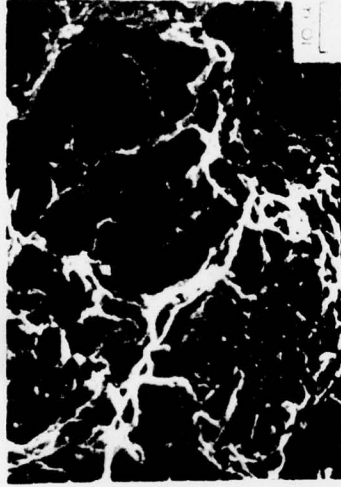
TESTED AT LIQD. N₂ TEMPERATURE (-196°C)

Figure - 8. Charpy impact fracture appearance of quenched and tempered ultra high purity 4340 type steel (B7) tested at 23°C and -196°C

TEMPERED AT : 200°C



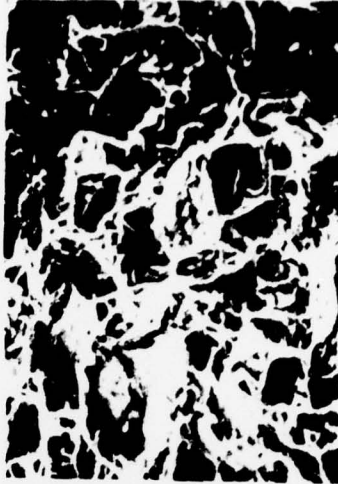
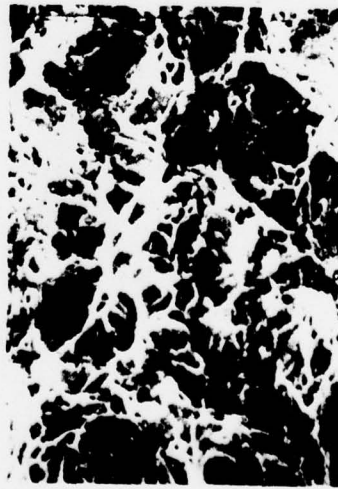
250°C



300°C



TESTED AT ROOM TEMPERATURE (23°C)



TESTED AT LIQD. N₂ TEMPERATURE (-196°C)

Figure -9. Charpy impact fracture appearance of quenched and tempered high purity 4340 steel (heat 840) tested at 23°C and - 196°C

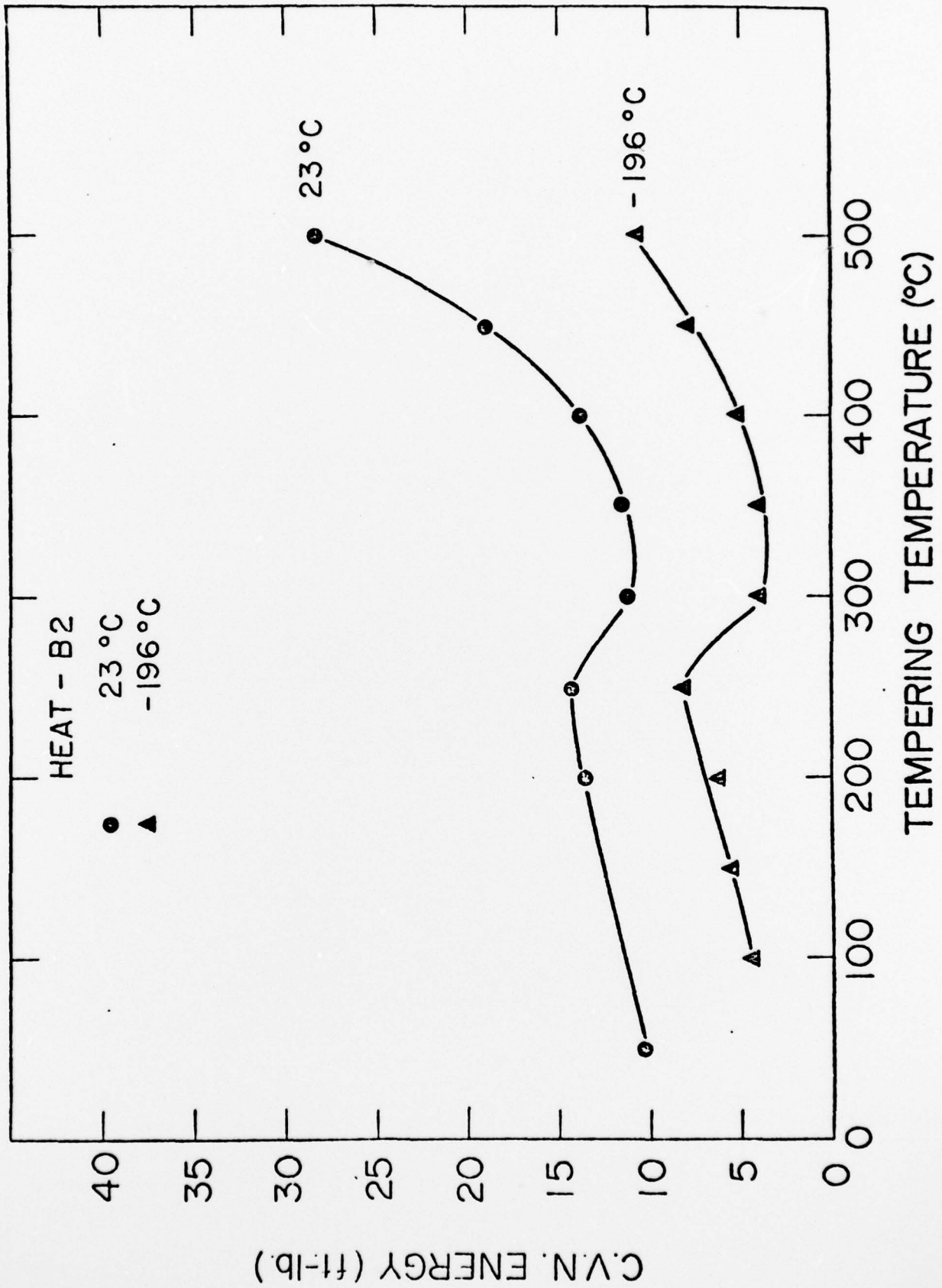
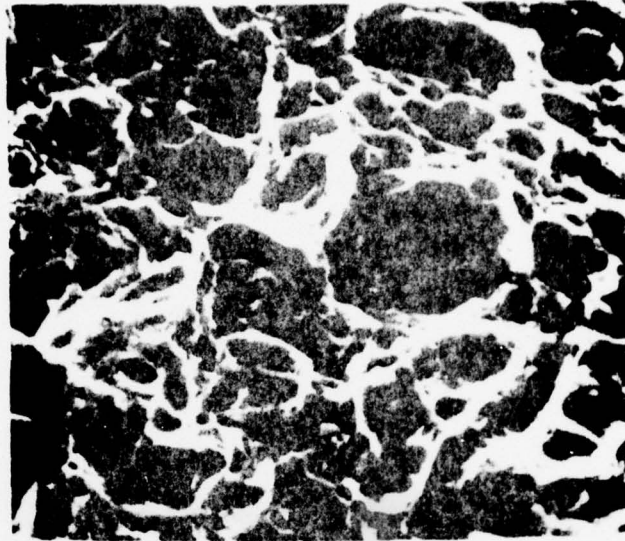
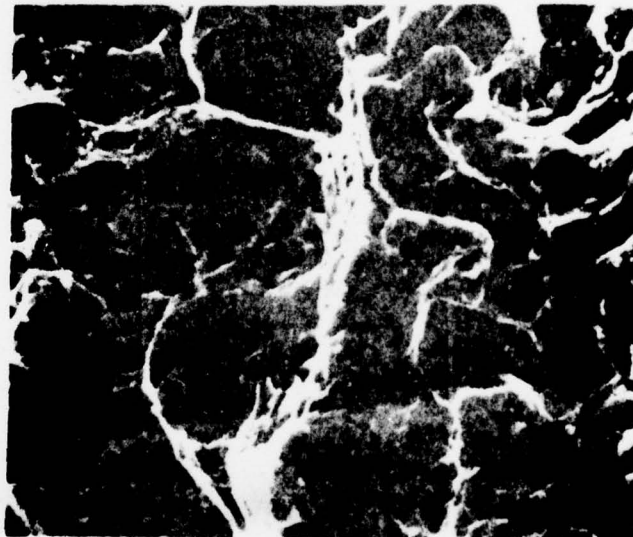


FIG.-10

TEMPERED AT 350°C



TESTED AT ROOM TEMP. (23°C)



TESTED AT LIQD. N₂ TEMP. (-196°C)

Figure-11. Charpy impact fracture appearance of quenched and tempered commercial 4340 type steel (B2) tested at 23°C and -196°C. 1500 x

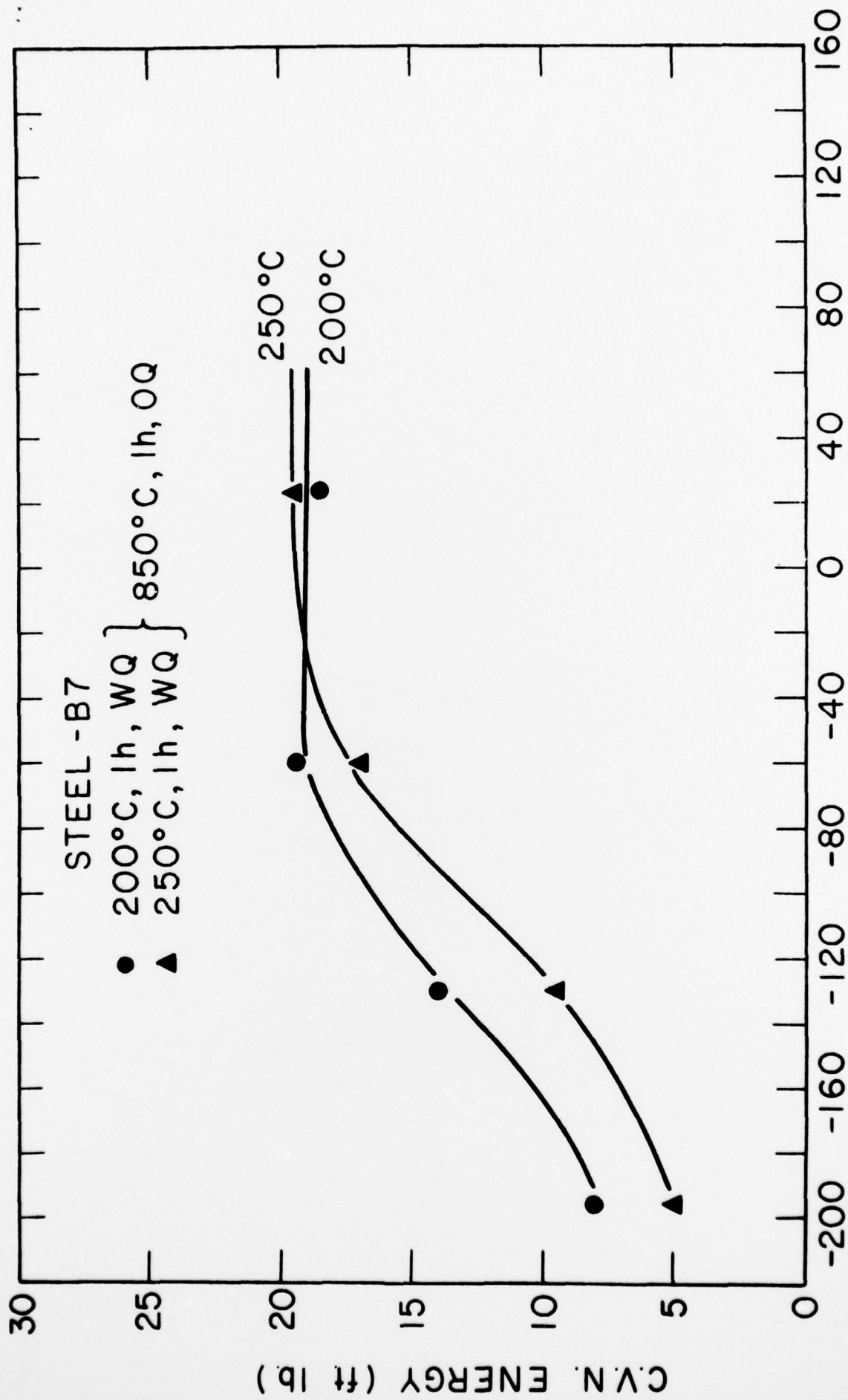
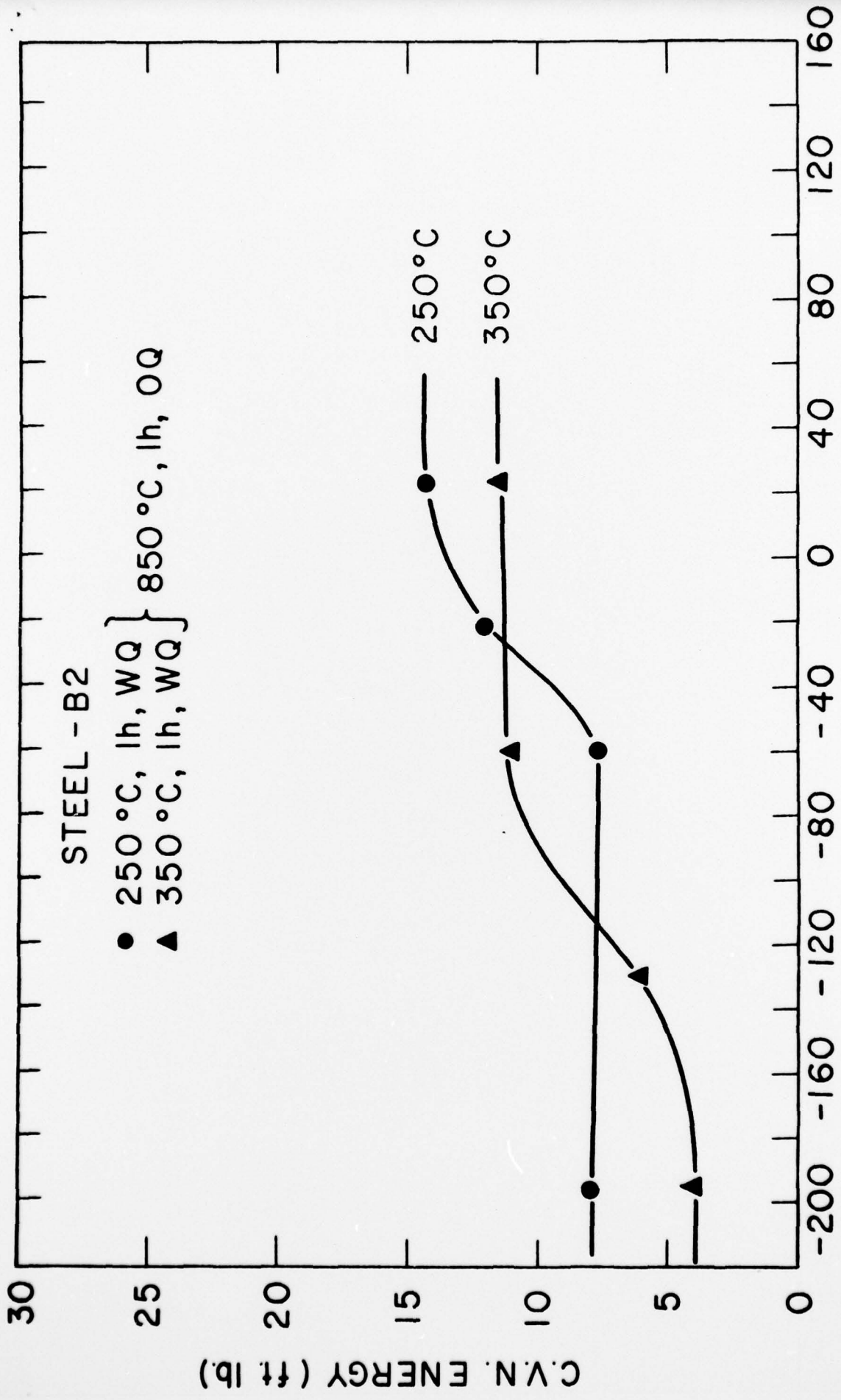


FIG-12



TESTING TEMPERATURE, °C

FIG-13

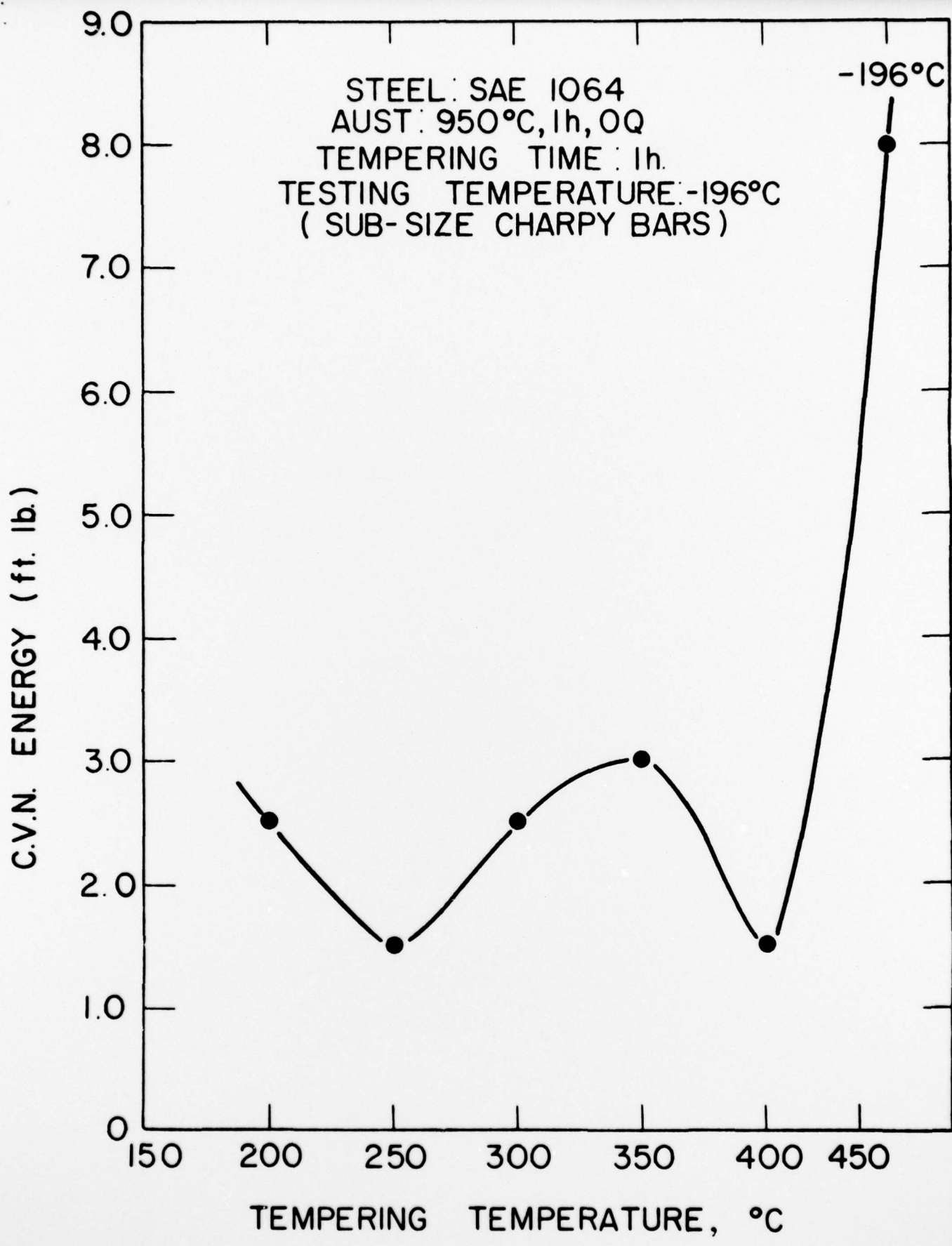


FIG. - 14

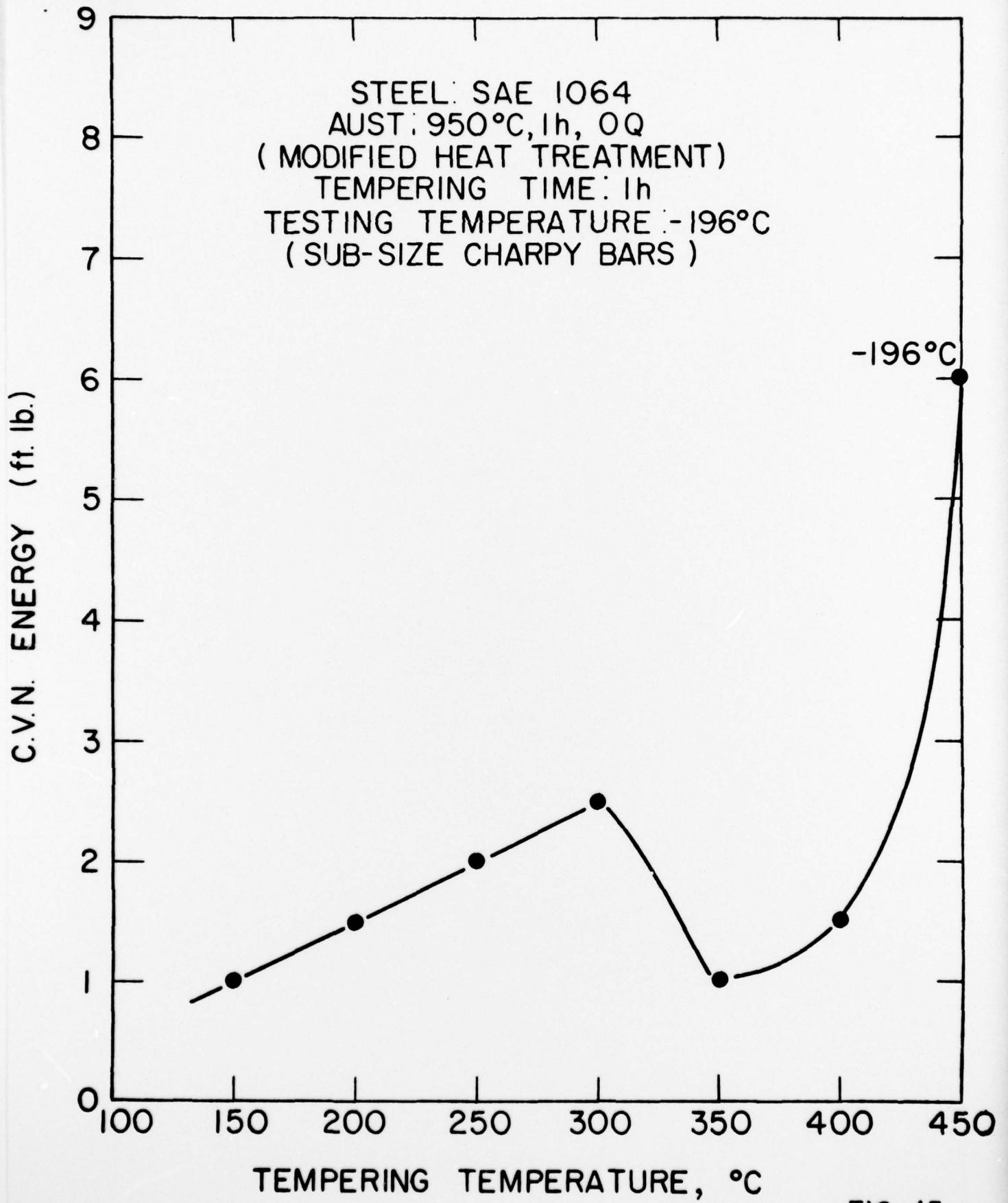


FIG.-15

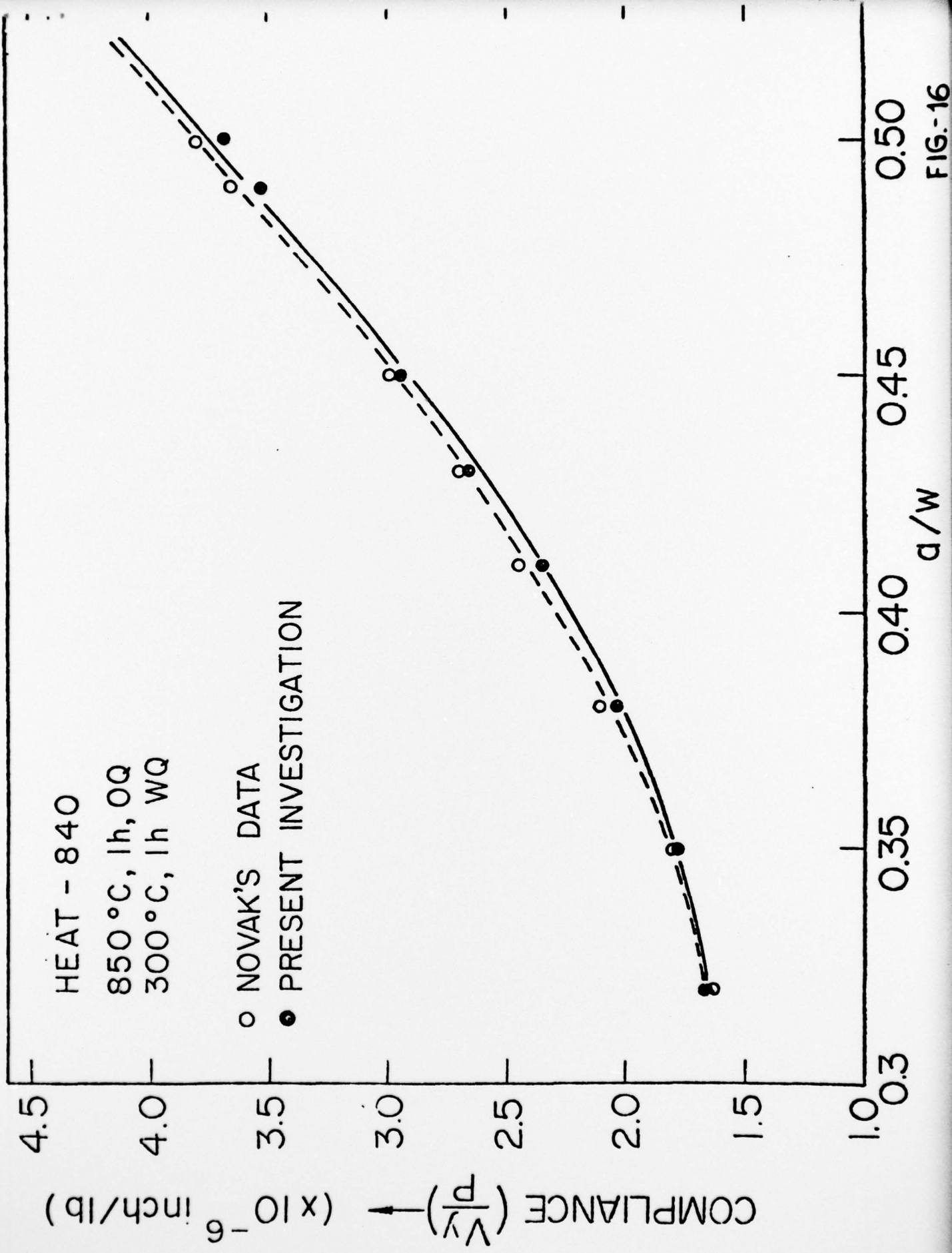
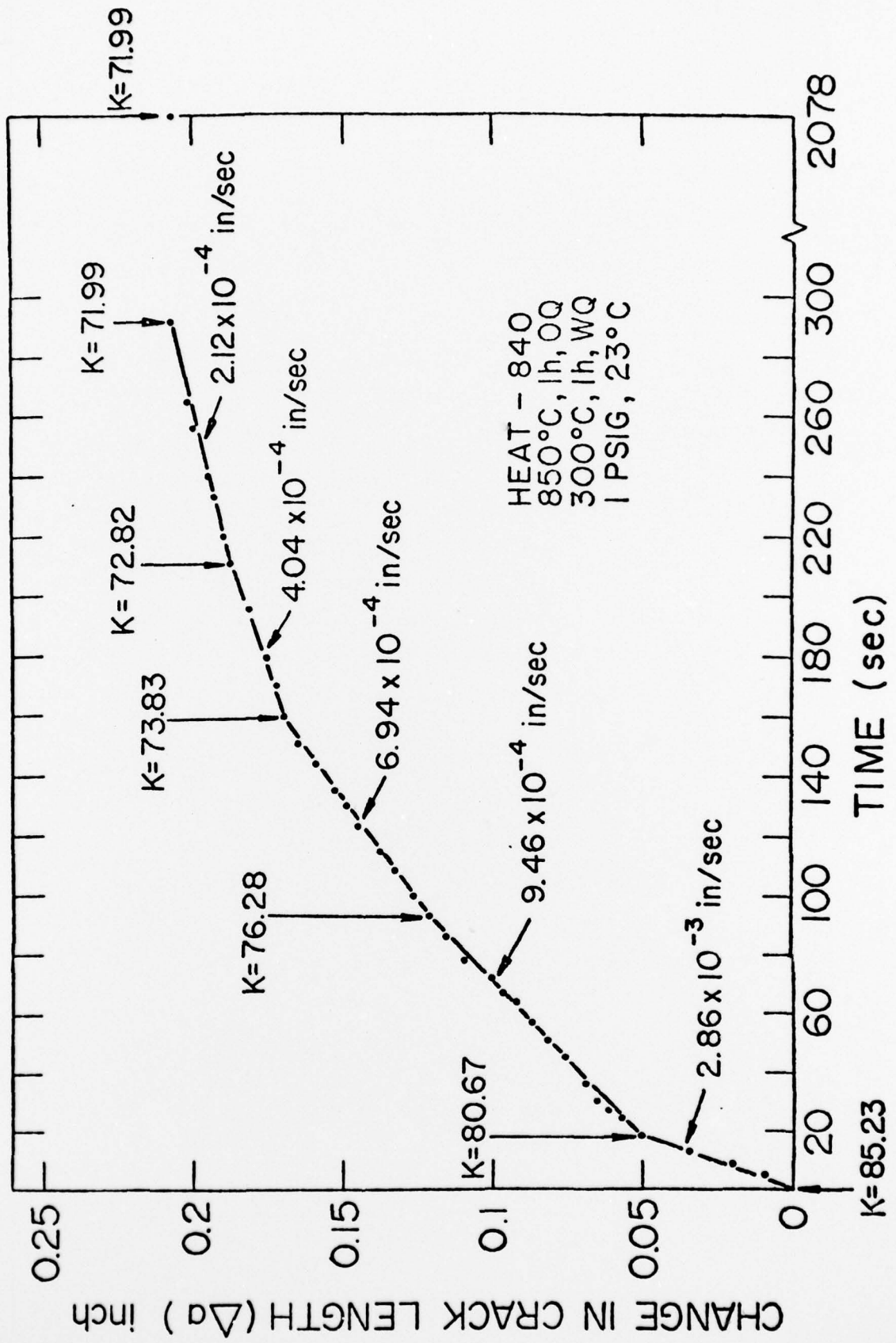


FIG.-16



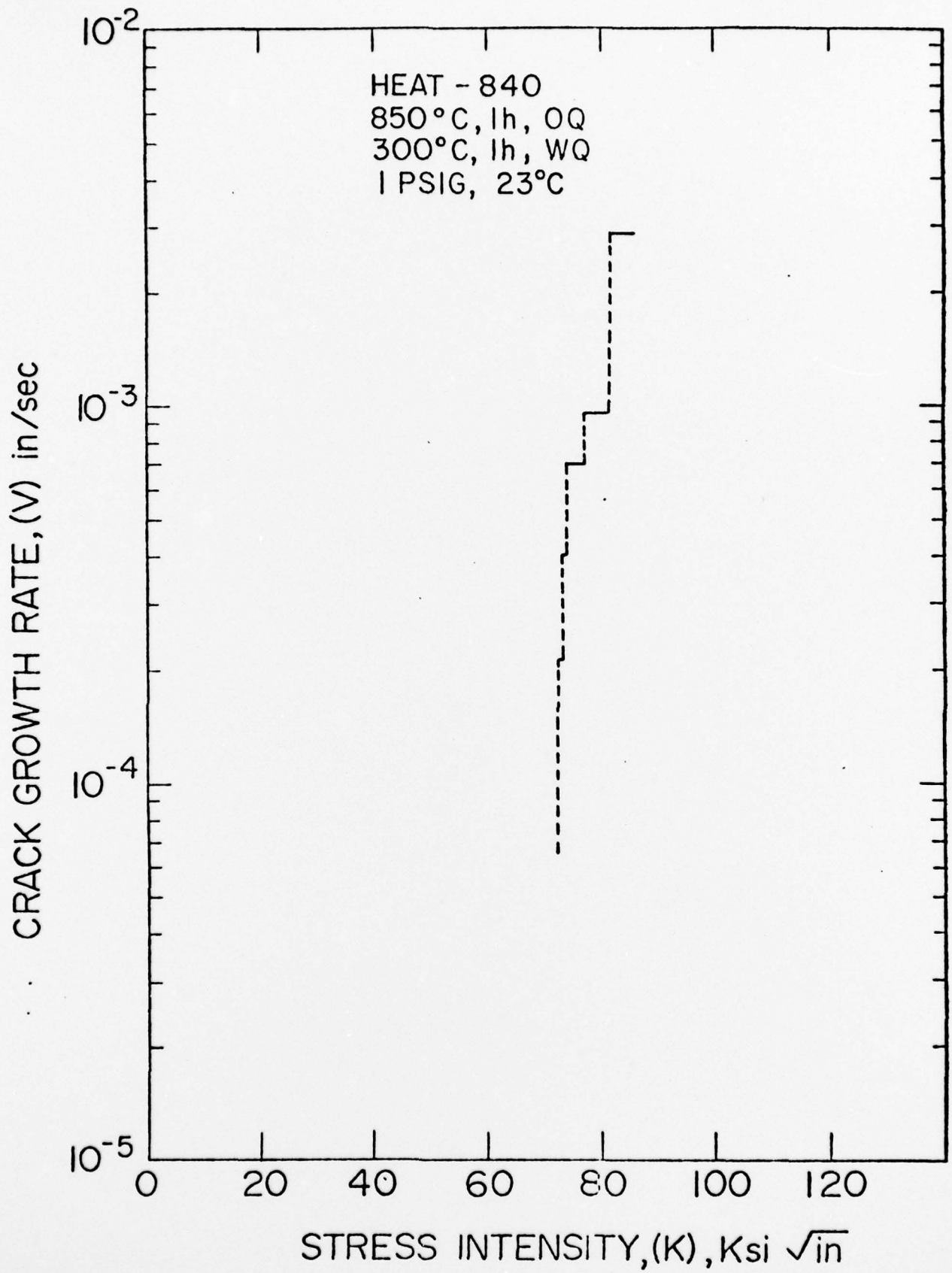


FIG.-18

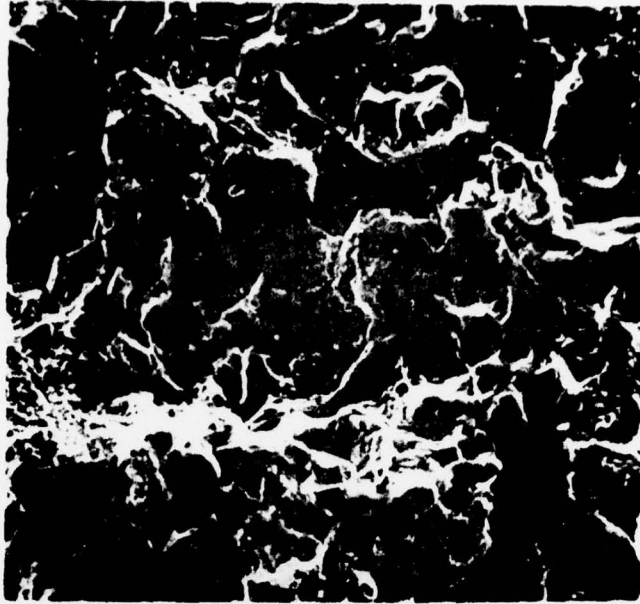


Figure-19. Fracture surface of WOL sample of heat 840 fractured in hydrogen showing intergranular fracture mode. 500 x



Figure-20. Fracture surface of pre-charged (H_2) SAM sample after slow bend test. 100 x